Experimental Study of Quantum Chaos with Cold Atoms

M. G. Raizen, V. Milner, W. H. Oskay, and D. A. Steck

Department of Physics, The University of Texas at Austin
Austin, Texas 78712-1081, USA

1. – Introduction.

The hallmark of classical chaos in the motion of an ensemble of particles is diffusive growth in momentum and position. A system of quantum particles, in contrast, was predicted by Casati *et al.* to diffuse in phase space only for a limited time, following the classical prediction [1]. The diffusion is predicted to cease after the "quantum break time" due to quantum interference, and the momentum distribution is predicted to become exponential. This striking effect, known as dynamical localization, has stimulated a great deal of interest and discussion since it was first predicted. Dynamical localization was predicted to occur in a wide range of systems, and was also shown to be closely related to Anderson localization, a suppression of electronic conduction in a disordered metal at low temperature.

Experimental observation of dynamical localization requires a globally chaotic (classical) phase space, because diffusion can also be restricted by residual stable islands and by classical boundaries according to the Kolmogorov–Arnol'd–Moser (KAM) theorem. The duration of the experiment must exceed the quantum break time, so that quantum effects can be manifested. Finally, the system must be sufficiently isolated from the environment that quantum interference effects can persist.

In these lectures we review our work on the motion of atoms in time-dependent potentials. In particular, we study momentum distributions of ultra-cold atoms that are exposed to time-dependent, one-dimensional dipole forces. As we will show, the typical potentials are highly nonlinear, so that the classical dynamics can become chaotic. Since dissipation can be made negligibly small in this system, quantum effects can become

© Società Italiana di Fisica

important.

The organization of the lectures is as follows. In section 2 we give a theoretical background on atomic motion in a far-detuned dipole potential, and provide a classical analysis of the potential in terms of nonlinear resonances. In section 3 we describe the general experimental approach. In section 4 we introduce the δ-kicked rotor, a paradigm for classical and quantum chaos, and describe our experimental realization, leading to the observation of dynamical localization. Finally, in section 5, we discuss some current and future work in this emerging field.

2. – A Two-Level Atom in a Standing-Wave Potential.

We begin our analysis by considering a two-level atom of transition frequency ω_0 interacting with a standing wave of near-resonant light. If the standing wave is composed of two counterpropagating beams, each with field amplitude E_0 and wavenumber $k_{\rm L} = 2\pi/\lambda_{\rm L} = \omega_{\rm L}/c$, then the atom is exposed to an electric field of the form $\vec{E}(x,t) = \hat{y}[E_0\cos(k_{\rm L}x)e^{-i\omega_{\rm L}t} + \text{c.c.}]$, and its Hamiltonian in the rotating-wave approximation is given by

$$H(x,p,t) = \frac{p^2}{2M} + \hbar\omega_0|\mathrm{e}\rangle\langle\mathrm{e}| + \left[\mu E_0\cos(k_{\rm L}x)e^{-i\omega_{\rm L}t}|\mathrm{e}\rangle\langle\mathrm{g}| + \text{H.c.}\right] \ . \tag{1}$$

Here $|\mathrm{g}\rangle$ and $|\mathrm{e}\rangle$ are the ground and excited internal states of the atom, x and p are its center-of-mass position and momentum, M is its mass, and μ is the electric dipole moment coupling the internal states.

Using standard techniques, we obtain two coupled Schrödinger equations for the ground, $\psi_{\rm g}(x,t)$, and excited, $\psi_{\rm e}(x,t)$ state amplitudes

$$i\hbar\frac{\partial\psi_{\rm g}(x,t)}{\partial t} = -\frac{\hbar^2}{2M}\frac{\partial^2}{\partial x^2}\psi_{\rm g}(x,t) + \frac{\hbar\Omega}{2}\cos(k_{\rm L}x)\psi_{\rm e}(x,t) \ , \tag{2}$$

$$i\hbar\frac{\partial\psi_{\rm e}(x,t)}{\partial t} = -\frac{\hbar^2}{2M}\frac{\partial^2}{\partial x^2}\psi_{\rm e}(x,t) + \frac{\hbar\Omega}{2}\cos(k_{\rm L}x)\psi_{\rm g}(x,t) + \hbar\delta_{\rm L}\psi_{\rm e}(x,t) \ , \tag{3}$$

where $\Omega/2 \equiv \mu E_0/\hbar$ is the Rabi frequency of an atom interacting with just one of the light beams. Note that spontaneous emission from the excited state is neglected; this approximation is valid for the case of large detunings $\delta_{\rm L} \equiv \omega_{\rm L} - \omega_0$ from the atomic resonance. The large detuning also permits an adiabatic elimination of the excited-state amplitude, resulting in a single equation for the ground-state amplitude

$$i\hbar\frac{\partial\psi_{\rm g}}{\partial t} = -\frac{\hbar^2}{2M}\frac{\partial^2}{\partial x^2}\psi_{\rm g} + \frac{\hbar\Omega^2}{4\delta_{\rm L}}\cos^2(k_{\rm L}x)\psi_{\rm g} \ . \tag{4}$$

The wavefunction of the now "structureless" atom obeys a Schrödinger equation with a one-dimensional Hamiltonian

$$H(x,p) = \frac{p^2}{2M} + V_0 \cos 2k_{\rm L} x \ . \tag{5}$$

The potential has a period of one-half the optical wavelength and an amplitude V_0 that is proportional to the intensity of the standing-wave and inversely proportional to its detuning:

$$V_0 = \frac{\hbar\Omega^2}{8\delta_{\rm L}} = \frac{\hbar(\Gamma/2)^2}{\delta_{\rm L}} \ \frac{I}{I_{\rm sat}} \ . \tag{6}$$

Here Γ is the linewidth of the transition and μ is its dipole matrix element. I is the intensity of each of the beams comprising the standing wave and $I_{\rm sat} \equiv \pi\hbar\omega_0\Gamma/3\lambda_{\rm L}^2$ is the saturation intensity for the transition ($I_{\rm sat} = 1.65$ mW/cm^2 for the case of cesium atoms interacting with far-detuned, linearly polarized light). Eq. (6) was derived for a standing wave composed of two counterpropagating beams of equal intensities. If the two beams are not perfectly matched the potential amplitude is still given by this equation, with I taken as the geometric mean of the two intensities.

The classical analysis of Eq. (5) is the same as for a pendulum or rigid rotor, except that the conjugate variables here are position and momentum rather than angle and angular momentum. To address the problem of quantum chaos, we must go beyond the pendulum or stationary standing wave by introducing time-dependent potential. The connection between atom optics and quantum chaos was first recognized by Graham *et al.* who proposed that dynamical localization could be observed in the momentum transfer of ultra-cold atoms in a phase-modulated standing wave of light [2]. More generally, as shown below, quantum chaos can be studied by adding an explicit time dependence to the one-dimensional Hamiltonian. This can be accomplished, for example, with a time-dependent amplitude or phase of the standing wave. The electric field of the standing wave then takes the form $\vec{E}(x,t) = \hat{y}[E_0 F_1(t)\cos\{k_{\rm L}[x - F_2(t)]\}e^{-i\omega_{\rm L}t} + c.c.]$. The amplitude and phase modulations in our experiments are slow compared to the parameters ω_0 and $\delta_{\rm L}$ relevant to the derivation of Eq. (5), so they change that equation by simply modifying the amplitude and phase of the sinusoidal potential. The generic time-dependent potential is thus

$$H(x,p,t) = \frac{p^2}{2M} + V_0 F_{\rm amp}(t) \cos\left[2k_{\rm L}x - F_{\rm ph}(t)\right] \ . \tag{7}$$

For simulations and theoretical analyses it is helpful to write Eq. (7) in dimensionless units. We take $x_{\rm u} = 1/2k_{\rm L}$ to be the basic unit of distance, so the dimensionless variable $\phi \equiv x/x_{\rm u} = 2k_{\rm L}x$ is a measure of the atom's position along the standing-wave axis. Depending on the time dependence of the interaction, an appropriate time scale $t_{\rm u}$ is chosen; the variable $\tau \equiv t/t_{\rm u}$ is then a measure of time in this unit. The atomic momentum is scaled accordingly into the dimensionless variable $\rho \equiv p\,t_{\rm u}/Mx_{\rm u} = p\,2k_{\rm L}t_{\rm u}/M$. This

transformation preserves the form of Hamilton's equations with a new (dimensionless) Hamiltonian $\mathcal{H}(\phi,\rho,\tau) = H(x,p,t)\cdot t_{\rm u}^2/Mx_{\rm u}^2 = H\cdot 8\omega_{\rm r}t_{\rm u}^2/\hbar$.

With this scaling, Eq. (7) can be written in the dimensionless form

$$\mathcal{H}(\phi,\rho,\tau) = \frac{\rho^2}{2} + k f_{\rm amp}(\tau)\cos\left[\phi - f_{\rm ph}(\tau)\right] \ . \tag{8}$$

The scaled potential amplitude is $k \equiv V_0\cdot 8\omega_{\rm r}t_{\rm u}^2/\hbar$. In these transformed variables, the Schrödinger equation in the position representation becomes

$$i\hbar\frac{\partial}{\partial\tau}\Psi(\phi,\tau) = \left[-\frac{\hbar^2}{2}\frac{\partial^2}{\partial\phi^2} + k f_{\rm amp}(\tau)\cos\left[\phi - f_{\rm ph}(\tau)\right]\right]\Psi(\phi,\tau) \ . \tag{9}$$

Here the dimensionless parameter $\hbar$ depends on the temporal scaling used in the transformation

$$\hbar \equiv 8\omega_{\rm r}t_{\rm u} \ . \tag{10}$$

In the transformation outlined here, the commutation relation between momentum and position becomes $[\phi,\rho] = i\hbar$. Thus $\hbar$ is a measure of the quantum resolution in the scaled phase space. Another general note on this transformation concerns the measure of the atomic momentum. Since an atom interacts with a near-resonant standing wave, its momentum can be changed by stimulated scattering of photons in the two counter-propagating beams. If a photon is scattered from one of these beams back into the same beam, the result is no net change in the atom's momentum. But if the atom scatters a photon from one of the beams into the other, the net change in its momentum is two photon recoils. The atom can thus exchange momentum with the standing wave only in units of $2\hbar k_{\rm L}$. In the transformed, dimensionless units, this quantity is

$$\frac{p}{2\hbar k_{\rm L}} = \frac{\rho}{\hbar} \ . \tag{11}$$

For a sample of atoms initially confined to a momentum distribution narrower than one recoil, the discreteness of the momentum transfer would result in a ladder of equally spaced momentum states. In our experiments the initial momentum distributions were significantly wider than two recoils, so the observed final momenta had smooth distributions rather than discrete structures.

3. – Experimental Method.

The experimental study of momentum transfer in time-dependent interactions consists of three main components: preparation of the initial conditions,exposure to the interaction potential, and measurement of atomic momentum. The initial distribution should ideally be narrow in position and momentum, and should be sufficiently dilute so that atom-atom interactions can be neglected. The time-dependent potential should be

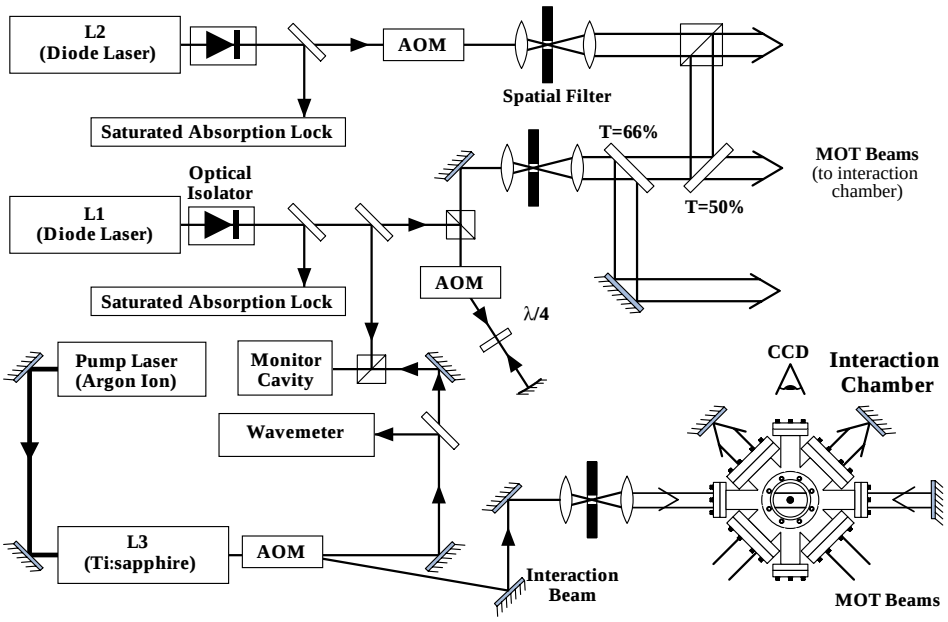

Fig. 1. – Schematic diagram of the experimental setup. Two diode lasers L1 and L2 provide the light for the MOT, and a Ti:sapphire laser L3 provides the far-detuned standing wave.

one-dimensional (for simplicity), with full control over the amplitude and phase. In addition, noise and coupling to the environment must be minimized to enable the study of quantum effects. Finally the measurement of final momenta after the interaction should have high sensitivity and accuracy. Using the tools of atom optics it is possible to realize all these conditions.

The first generation of our experiments was performed with laser-cooled sodium atoms [3, 4, 5, 6]. We describe here the second generation apparatus that uses laser-cooled cesium atoms instead of sodium and has many advantages in terms of experimental control and signal-to-noise. A schematic of the experiment is shown in Fig.1. The starting point for the experiments are laser-cooled cesium atoms in a magneto-optic trap (MOT) [7]. Two actively locked single-mode diode lasers (L1, L2) at 852 nm are used for cooling, trapping, and detection of the cesium atoms. The main beam from L1 is double passed through a tunable acousto-optic modulator (AOM) that provides fast control over the intensity and detuning of the beam. During the trapping stage of the experiment, the light from L1 is locked 15 MHz to the red of the $(6S_{1/2}, F = 4) \longrightarrow (6P_{3/2}, F = 5)$ cycling transition. This light is collimated with a waist of 1.1 cm and has a typical power of 23 mW at the chamber. The light from L1 is split into three beams that are retroreflected through the center of the chamber in a standard six-beam MOT configuration. The second laser, L2, prevents optical pumping into the $F = 3$ ground state during the

trapping and detection stages.

After trapping and initial cooling, the intensity of L1 is reduced for 7 ms and the detuning is increased to 55 MHz to further cool the sample. After this final cooling, the trapping fields are turned off, while the light from L2 is left on for additional 150 μs to optically pump the atoms to the $(6S_{1/2}, F = 4)$ ground state. Typically, we trap 10^6 atoms with $\sigma_x = 0.15\,\mathrm{mm}$ and $\sigma_p/2\hbar k_\mathrm{L} = 4$. Once the trapping light is off, the interaction potential is turned on. The time-dependent standing wave is provided by a stabilized single-mode Ti:sapphire laser (L3). The light from L3 passes through an acousto-optic modulator that controls the temporal profile of the standing wave. The linearly polarized beam is spatially filtered, aligned with the atoms, and retroreflected through the chamber to form a standing wave.

After the interaction with the time-dependent nonlinear potential, the atomic momentum is measured using an in-situ time-of-flight technique that we developed. The atoms expand ballistically for a controlled duration (typically 15 ms) and their motion is then frozen by turning on optical molasses. The atomic position is recorded via fluorescence imaging in a short (10 ms) exposure on a cooled CCD. The final spatial distribution and the free-drift time enable the determination of the one-dimensional momentum distribution. The systematic uncertainties in the determination of the momentum distributions include the spatial calibration of the imaging system and the ambiguity in the drift time due to motion occurring during different interaction times, giving an overall systematic uncertainty of $\pm 2\%$ in the momentum measurements.

4. – Kicked Rotor.

The classical δ-kicked rotor, or the equivalent standard mapping, is a textbook paradigm for Hamiltonian chaos. A mechanical realization would be an arm rotating about a pivot point. The rotation is free, except for sudden impulses that are applied periodically. The Hamiltonian for the problem is given by

$$\mathcal{H} = \frac{\rho^2}{2} + K\cos\phi \sum_{n=-\infty}^{\infty} \delta(\tau - n)\ . \tag{12}$$

The evolution consists of resonant-kicks that are equally spaced in time, with free motion in between. The quantity K is called the stochasticity parameter, and is the standard control parameter for this system. As K is increased, the size of each resonant kick grows. Beyond a threshold value of $K \approx 1$ it has been shown that phase space is globally chaotic [8].

The quantum version of this problem has played an equally important role for the field of quantum chaos since the pioneering work of Casati et al. [1] and Chirikov [9]. In particular, dynamical localization was predicted to occur for the kicked rotor and detailed scaling laws were derived. Although this model may seem unique, many physical systems can be mapped locally onto the kicked rotor, so that it is actually a universal paradigm system.

To observe dynamical localization in an experimental realization of the kicked rotor, we turned the standing wave on and off in a series of N short pulses with period T. This system differs from the ideal kicked rotor in two ways. The first difference is that the conjugate variables here are position and momentum instead of angle and angular momentum, so that strictly speaking our system consists of kicked *particles*. The second is that the pulses have finite duration instead of being δ-kicks. The effect of finite pulse duration was also considered by Blümel *et al.* [10] in the context of molecular rotation excitation. The first distinction might seem problematic, because there is a natural quantization of angular momentum, in contrast to a continuum of momentum states for a free particle. In our system, however, the quantization of momentum is imposed by the periodicity of the wells, so that the momentum kicks must occur in units of two recoils. The initial distribution, on the other hand, can be continuously distributed over different momentum states, providing averaging of diffusion and localization. The effects of finite pulse duration are analyzed below, but we note here that if the atoms do not move significantly compared to the spatial period during a pulse, this system is an excellent approximation of the δ-kicked rotor.

Atomic motion in this case can be described by the Hamiltonian of Eq. (7) with $F_{\rm amp} = \sum_{n=1}^{N} F(t - nT)$ and $F_{\rm ph} = 0$,

$$H = \frac{p^2}{2M} + V_0 \cos(2k_{\rm L}x) \sum_{n=1}^{N} F(t - nT) \ . \tag{13}$$

Here the function $F(t)$ is a narrow pulse in time centered at $t = 0$ that modulates the intensity of the standing wave. The sum in this equation represents the periodic pulsing of the standing wave amplitude by multiplying V_0 with a value in the range $0 \le F(t) \le 1$.

With the scaling introduced in Section II and the unit of time taken to be T, the period of the pulse train, the Hamiltonian for this system becomes

$$\mathcal{H} = \frac{\rho^2}{2} + K \cos\phi \sum_{n=1}^{N} f(\tau - n) \ . \tag{14}$$

The train of δ-functions in Eq. (12) has been replaced here by a series of normalized pulses $f(\tau) = F(\tau T)/\int_{-\infty}^{\infty} F(\tau T) d\tau$. Note that the scaled variable $\tau = t/T$ measures time in units of the pulse period. As described earlier, $\phi = 2k_{\rm L}x$ is a measure of an atom's displacement along the standing wave axis and ρ is its momentum in units of $2\hbar k_{\rm L}/\hbar$.

Aside from the temporal profile of the pulses, all the experimental parameters that determine the classical evolution of this system are combined into one quantity, the stochasticity parameter K. As we will see, the quantum evolution depends additionally on the parameter $\hbar$. These two dimensionless quantities thus characterize the dynamics of Eq. (14). In terms of the physical parameters of Eq. (13), they are

$$K \equiv 8V_0\eta T\omega_{\rm r}/\hbar \ \ , \tag{15}$$

$$\hbar = 8\omega_{\rm r} T \ . \tag{16}$$

Here $t_{\rm p}$ is the FWHM duration of each pulse, and $\eta \equiv \int_{-\infty}^{\infty} F(t)dt \propto t_{\rm p}$ is the pulse integral. Atoms with low velocities do not move significantly during the pulse, so their classical motion can be described by a map. By integrating Hamilton's equations of motion over one period, we obtain the change in an atom's displacement and momentum:

$$\begin{aligned} \Delta\phi &= \int_n^{n+1} dt\ \rho = \rho \ , \\ \Delta\rho &= \int_n^{n+1} dt\ K \sin\phi \sum f(\tau - n) = K \sin\phi \ . \end{aligned} \tag{17}$$

The discretization of these relations is the classical map,

$$\begin{aligned} \phi_{n+1} &= \phi_n + \rho_{n+1} \ , \\ \rho_{n+1} &= \rho_n + K \sin\phi_n \ , \end{aligned} \tag{18}$$

that is known as the "standard" map [8]. For small values of K, the phase space of this system shows bounded motion with regions of local chaos. Global stochasticity occurs for values of K greater than ~ 1, and widespread chaos appears at $K > 4$, leading to unbounded motion in phase space. Correlations between kicks in the spatial variable ϕ can be ignored for large values of K, so this map can be iterated to estimate the diffusion constant. After N kicks, the expected growth in the square of the momentum is

$$\langle (\rho_N - \rho_0)^2 \rangle = K^2 \sum_{n=0}^{N-1} \langle \sin^2 \phi_n \rangle + K^2 \sum_{n \neq n'}^{N-1} \langle \sin\phi_n \sin\phi_{n'} \rangle \tag{19}$$

$$\cong \frac{K^2}{2} N \ . \tag{20}$$

The diffusion in momentum is thus

$$\langle \rho^2 \rangle = DN, \quad \text{with } D \equiv \frac{K^2}{2}. \tag{21}$$

Note that this description, which follows from the discretization into the standard map, requires the duration of the pulses to be short. To understand the effects of a finite pulse-width, consider the case where the pulse profile $f(\tau)$ is Gaussian with an RMS width τ_0. In the limit of a large number of kicks N, the potential in Eq. (14) can be expanded into a Fourier series:

$$\begin{aligned} \mathcal{H} &= \frac{\rho^2}{2} + K \cos\phi \sum_{m=-\infty}^{\infty} e^{im2\pi\tau} e^{-(m2\pi\tau_0)^2/2} \\ &= \frac{\rho^2}{2} + \sum_{m=-\infty}^{\infty} K_m \cos(\phi - m2\pi\tau) \end{aligned} \tag{22}$$

with

$$K_m \equiv K \ \exp\left[-(m2\pi\tau_0)^2/2\right] \ . \tag{23}$$

The nonlinear resonances are located (according to the stationary phase condition) at $\rho = d\phi/d\tau = m2\pi$. This expansion is similar to the resonance structure of the δ-kicked rotor, in which the K_m are constant for all values of m. In Eq. (22), however, the widths of successive resonances fall off because of the exponential term in the effective stochasticity parameter K_m. This fall-off is governed by the pulse profile; the result of Eq. (22) was derived for the case of a Gaussian pulse shape, but in general K_m is given by the Fourier coefficients of the periodic pulse train.

The nonzero pulse widths thus lead to a finite number of significant resonances in the classical dynamics, which in turn limits the diffusion that results from overlapping resonances to a band in momentum. The width of this band can be made arbitrarily large by decreasing the pulse duration and increasing the well depth, thereby approaching the δ-function pulse result. This can be seen in the result derived above. In the limiting case of $\tau_0 \to 0$ with K fixed (infinitesimal pulse width and large well depth), we recover the resonance structure expected for the δ-function limit in Eq. (12): $K_m = K$. In the experiment, the pulse width only needs to be small enough that the band of diffusion is significantly wider than the range of final momenta and that the effective diffusion constant K_m is approximately uniform over this range.

An example of the bounded region of chaos that arises from the finite pulse duration ($t_{\rm p}$) is illustrated in Fig. 2, which shows classical phase portraits for the δ-kicked rotor (Fig. 2(a)) and two square-pulse cases (Fig. 2(b) and (c)). The phase portrait of Fig. 2(b) is typical for our current cesium experiment, and the boundaries are well outside the range of detectable atomic momenta, $|p/2\hbar k_{\rm L}| \leq 80$.

The boundary in momentum can also be understood using the concept of an impulse. If the atomic motion is negligible while the pulse is on, the momentum transfer occurs as an impulse, changing the momentum of the atom without significantly affecting its position. Atoms with a sufficiently large velocity, however, can move over several periods of the potential while the pulse is on. The impulse for these fast atoms is thus averaged to zero, and acceleration to larger velocities is inhibited. The result is a momentum boundary that can be pushed out by making each pulse shorter.

Classically, then, the atoms are expected to diffuse in momentum until they reach the momentum boundary that results from the finite pulse width. Equation (21) indicates that the energy of the system $\langle \frac{1}{2}(p/2\hbar k_{\rm L})^2 \rangle$ thus grows linearly in time. In terms of the number of pulses N, this energy is

$$\left\langle \frac{1}{2}\left(\frac{p}{2\hbar k_{\rm L}}\right)^2 \right\rangle = \left\langle \frac{1}{2}\left(\frac{\rho}{\bar{k}}\right)^2 \right\rangle = \frac{1}{2\bar{k}^2}\frac{K^2}{2}N \ . \tag{24}$$

This system can be expected to exhibit quantum behaviors that are very different from those predicted classically. A quantum analysis of this system starts with the

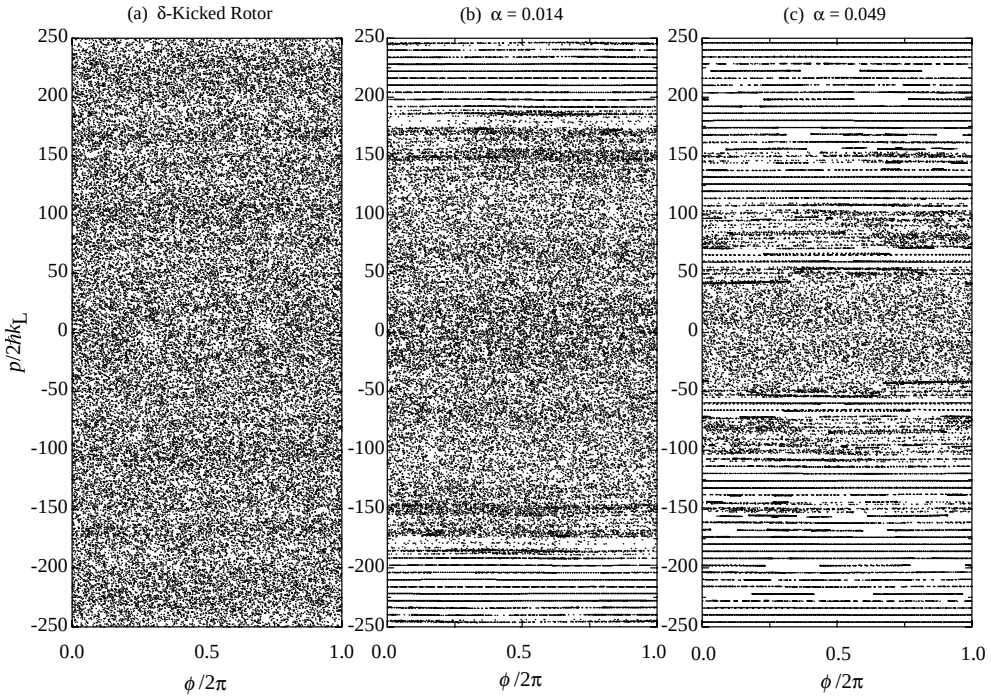

Fig. 2. – Classical phase portraits for the kicked rotor with $K = 10.5$, comparing δ-kicks (a) to square pulses of dimensionless widths $\alpha = t_{\rm p}/T = 0.014$ (b) and $\alpha = t_{\rm p}/T = 0.049$ (c). Case (b) is typical for our localization experiments. This case mimics the δ-kicked rotor for a momentum region much larger than used in our experiment ($|p/2\hbar k_{\rm L}| \leq 80$).

Schrödinger equation, Eq. (9). For the pulsed modulation of Eq. (14), this becomes

$$i\bar{k}\frac{\partial}{\partial\tau}\Psi(\phi,\tau) = \left[\frac{-\bar{k}^2}{2}\frac{\partial^2}{\partial\phi^2} + K\cos\phi\sum_n f(\tau - n)\right]\Psi(\phi,\tau)\ . \tag{25}$$

The periodic time dependence of the potential implies that the orthogonal solutions to this equation are time-dependent Floquet states. This system has been studied extensively in the ideal case of $f(\tau) = \delta(\tau)$ with an infinite train of kicks ($n = 0, \pm1, \pm2, ...$) [1]. An analysis of this system by Chirikov et al. [9] shows that this system diffuses classically only for short times during which the discrete nature of the Floquet states is not resolved. As shown by Fishman *et al.* [11], Eq. (25) can be transformed into the form of a tight-binding model of condensed-matter physics. An analysis of that system indicates that the Floquet states of Eq. (25) are discrete and exponentially localized in momentum. Since these states form a complete basis for the system, the initial condition of an atom in the experiments can be expanded in a basis of Floquet states. Subsequent

diffusion is limited to values of momentum covered by those states that overlap with the initial conditions of the experiment. If the initial conditions are significantly narrow in momentum, the energy of the system should grow linearly with the number of kicks N, in agreement with the classical prediction in Eq. (24), until a "quantum break time" N^*. After this time, the momentum distribution approaches that of the Floquet states that constituted the initial conditions, and the linear growth of energy is curtailed. This phenomenon is known as dynamical localization.

We now describe our experimental results. We subjected the cooled and trapped atoms to a periodically pulsed standing wave and recorded the resulting momentum distributions. The beam had a typical power of 470 mW at the chamber and a waist of 1.44 mm. For all the experiments described here we detune this beam 6.1 GHz to the red of the cycling transition, with typical fluctuations of about 100 MHz. The pulse sequence consists of a series of 295 ns (FWHM) pulses with a rise/fall time of 70 ns and less than 3 ns variation in the pulse duration. The period was 20 μs with less than 4 ns variation. This period corresponds to $\bar{k} = 2.08$. The number of pulses and pulse period were computer-controlled with an arbitrary waveform generator. To study the temporal evolution of the atomic sample under the influence of the periodic kicks, these experiments were repeated with increasing numbers of kicks (N) with the well depth, pulse period, and pulse duration fixed. These successive measurements provided the momentum distributions at different times in the atomic sample's evolution. Such a series of measurements is shown in fig. 3. The distributions clearly evolve from an initial Gaussian at $N = 0$ to an exponentially localized distribution after approximately $N = 8$ kicks. We have measured distributions out until $N = 68$ and find no further significant change.

5. – Current and Future Directions

Our recent work has focused on the effects of noise and dissipation on dynamical localization. To study the effects of noise, we replace the fixed kick amplitude k with a random, step-dependent kick amplitude k_n, to introduce amplitude noise in the kicks. To induce dissipation, we add a weak, resonant interaction that will induce a small number of spontaneous scattering events, primarily between kicks. In both cases we observe the destruction of localization and a transition to classical (Gaussian) distributions [12]. We are now doing a comparative study of the sensitivity of the quantum system to different types of noise and dissipation in an effort to understand decoherence in this system.

Another direction in our group has been to study quantum transport in a regime of classical anomalous diffusion. This occurs for certain values of the stochasticity parameter and is associated with accelerator modes in classical phase space. In that regime we observe large energy growth with no evidence for exponential localization [13].

The focus of this work has so far been on cases where the classical phase space is globally chaotic. The more generic situation in nature is a mixed phase space, consisting of islands of stability surrounded by regions of chaos. To study this regime, better initial conditions are needed. We have developed a new method which should enable

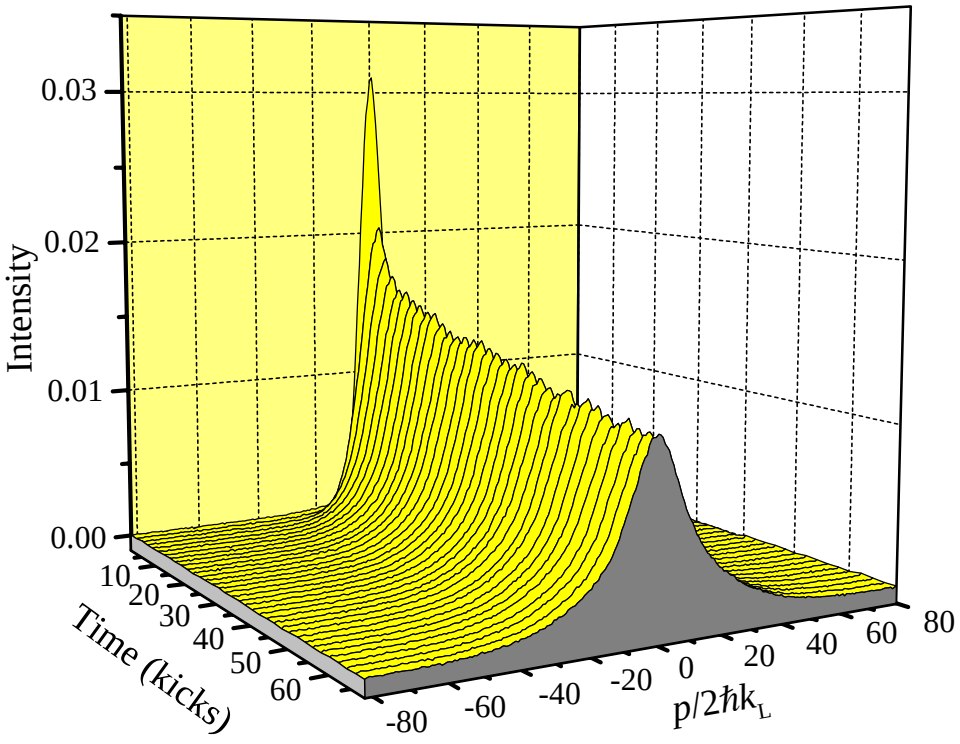

Fig. 3. – Time evolution of a typical kicked-rotor experiment for $K = 11.5 \pm 10\%, T = 20\mu$s, 0.283 μs pulse width, and $\bar{k} = 2.08$. The initial distribution is nearly Gaussian with $\sigma_p/2\hbar k_{\rm L} = 4.4$. The final distribution is exponential. The vertical axis is linear and in arbitrary units. The time increment between distributions is 2 kicks.

the preparation of a minimum-uncertainty "box" in phase space, and plan to implement this technique in our cesium experiment. This would enable a detailed study of quantum transport in mixed phase space.

REFERENCES

[1] Casati G., Chirikov B. V., Izrailev F. M. and Ford J., Stochastic Behaviour in Classical and Quantum Hamiltonian Systems, in *Lecture Notes in Physics*, Vol. **93**, edited by G. Casati and J. Ford (Springer-Verlag, Berlin) 1979, p. 334.
[2] Graham R., Schlautmann M., and Zoller P., *Phys. Rev. A*, **45** (1992) R19.
[3] Moore F. L., Robinson J. C., Bharucha C., Williams P. E., and Raizen M. G., *Phys. Rev. Lett.*, **73** (1994) 2974.

[4] Robinson J. C., Bharucha C., Moore F. L., Jahnke R., Georgakis G. A., Niu Q., Raizen M. G., and Sundaram B., *Phys. Rev. Lett.*, **74** (1995) 3963.
[5] Moore F. L., Robinson J. C., Bharucha C., Sundaram B., and Raizen M. G., *Phys. Rev. Lett.*, **75** (1995) 4598.
[6] Raizen M. G., *Advances in Atomic, Molecular, and Optical Physics*, **41** (1999) 43.
[7] Chu S., *Science*, **253** (1991) 861.
[8] Reichl L. E., *The Transition to Chaos in Conservative Classical Systems: Quantum Manifestations* (Springer-Verlag, Berlin) 1992, and references therein.
[9] Chirikov B. V., *Phys. Rep.*, **52** (1979) 265.
[10] Blümel R., Fishman S., and Smilansky U., *J. Chem. Phys.*, **84** (1986) 2604.
[11] Fishman S., Grempel D. R., and Prange R. E., *Phys. Rev. Lett.*, **49** (1982) 509.
[12] Klappauf B. G., Oskay W. H., Steck D. A. and Raizen M. G., *Phys. Rev. Lett.*, **81** (1998) 1203.
[13] Klappauf B. G., Oskay W. H., Steck D. A. and Raizen M. G., *Phys. Rev. Lett.*, **81** (1998) 4044.